Rigorous Analysis of the GTEM Cell

Roberto De Leo, T. Rozzi, *Fellow, IEEE*, Carlo Svara, and Leonardo Zappelli

Abstract—**This work deals with the modeling of the new GTEM cell, recently in use for field measurements, which consists of a tapered rectangular waveguide loaded with an eccentric sloping plate conductor. We derive the fields of the cross section of the uniform structure by transverse resonance diffraction and apply the "local modes" approach to the study of the longitudinal field distribution. The first few modes of the cell are obtained. Numerical results agree with those in the literature, where available. The treatment is highly accurate and requires no more computer power than that of a desktop computer.**

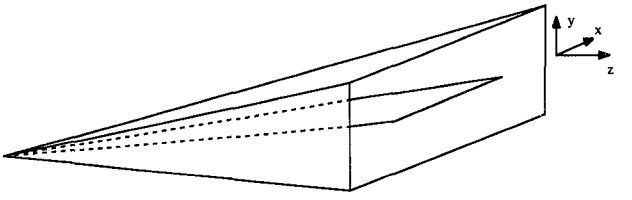

Fig. 1. The GTEM cell.

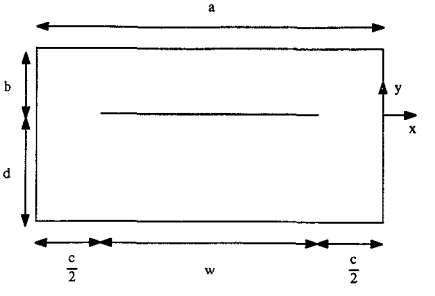

Fig. 2. The cross section.

I. Introduction

THE TEM cell is a fundamental tool in electromagnetic compatibility in that it permits one to simulate the effects of a plane wave incident on equipment under test in a region large with respect to the wavelength where the field is strictly TEM. The main restriction to the high-frequency operation of the cell arises from the cutoff of the first higher order mode. The new GTEM cell, shown in Fig. 1, permits one to overcome this restriction [1]–[3]. In fact, the absence of edges on the external surface, its tapering, and the use of absorbing material on the end wall ought to ensure operation up to frequencies of several GHz.

As regards the uniform (i.e., without tapering) TEM cell, many works in the literature study the distribution of the fundamental mode. The higher order modes were investigates some years ago in [4], where the first higher order mode was treated as a perturbation to the TE_{10} mode in a rectangular waveguide. In the same work, a comparison was made with the results obtained considering the TEM cell as a shielded stripline [5]. While in [4] only TE modes were considered, as TE_{10} is the main first higher order mode, later work included both polarizations [6]. The static capacitance of the line was also reported in [7].

In the present work, we study first the propagation in a uniform rectangular waveguide with an asymmetrically located inner plate in order to obtain as compactly as possible the modes of a guide of uniform cross section. Attention is then given to the propagation in a structure with tapered cross section as in the GTEM cell. In the first part, we use transverse resonance diffraction (TRD) [8], taking into account the presence of the edges of the inner plate. Our results for the uniform section show good agreement with results reported in [4] and [5], with very limited computer effort.

The second part deals with the analysis of propagation on GTEM structures, using "local modes" as in [9] but in more general form. This method describes propagation in a nonuniform guide through coupling of the modes of the guide of uniform cross section that is locally tangent to the nonuniform one (local modes). Hence, we obtain generalized telegraphist's equations, describing the interaction between modes of propagation. Coupling between modes and power transfer are examined and the frequency range for propagation of the TEM mode is determined.

Manuscript received May 31, 1990; revised October 3, 1990.

R. De Leo, T. Rozzi, and L. Zappelli are with the Departimento di Elettronica ed Automatica, Universita di Ancona, 60131 Ancona, Italy.

C. Svara was with the Departimento di Elettronica ed Automatica, Universita di Ancona, Ancona, Italy. He is now with Aeritalia SpA, Torino, Italy.

IEEE Log Number 9041948.

II. Local Modes

The analysis of this problem starts from the study of the local section of the GTEM structure. Here we develop the analysis by means of TRD, applied to TE and TM modes. The local section is represented in Fig. 2. Note that in this analysis, we consider the asymmetric position of the inner plate. Moreover, we take into account the presence of the edges at $x = -c/2$ and $x = -a + c/2$, where the fields orthogonal to the edges present a singularity of the type $r^{-1/2}$. We consider, moreover, symmetric structures along the x-direction, so that we may place electric and magnetic walls at $x = -a/2$ and study only half the structure along x.

A. TE Modes

The fields of the kth mode (apart from a normalization coefficient) are

$$\boldsymbol{h}_k(x,y) = -\frac{1}{k_t}\nabla_t \Pi_k(x,y)$$

$$\boldsymbol{e}_k(x,y) = -\frac{1}{k_t}\nabla_t \Pi_k(x,y)\times \hat{z}$$

$$h_{zk}(x,y) = \frac{k_t}{j\omega\mu}\Pi_k(x,y)$$

$$k_t^2 = k_0^2 - \beta^2 = -\partial_x^2 - \partial_y^2$$

$$\nabla_t^2 \Pi_k(x,y) + k_t^2 \Pi_k(x,y) = 0$$

with boundary conditions $\partial\Pi_k(x,y)/\partial x = 0$ at $x = 0$ and $x = -a$, $\partial\Pi_k(x,y)/\partial_y = 0$ at $y = -d$ and $y = b$. With these conditions, we write

$$h_{zk}(x,y) = \frac{k_t}{j\omega\mu}\sum_n \Phi_n(x) V_n \begin{cases} -\dfrac{\cos k_n(y-b)}{\sin k_n b}, & y \geqslant 0 \\ \dfrac{\cos k_n(y+d)}{\sin k_n d}, & y \leqslant 0 \end{cases}$$

with

$$\Phi_n(x) = \frac{2\delta_n}{\sqrt{a}}\cos\left(\frac{n\pi}{a}x\right), \qquad \delta_n = \begin{cases} \dfrac{1}{2}, & n = 0 \\ \dfrac{1}{\sqrt{2}}, & n \neq 0. \end{cases}$$

If n stands for $0,2,4,\cdots$, there is an electric wall at $x = -a/2$; if n stands for $1,3,5,\cdots$, there is a magnetic wall at $x = -a/2$ instead.

We can express the h_{zk} field component in terms of e_{xk} and evaluate the following admittance operators of the upper and lower half-spaces [8], respectively:

$$h_{zk}(x,0^+) = \hat{Y}_u \cdot e_{xk}(x,0) \equiv \int_{-c/2}^{0} Y_u(x,x') e_{xk}(x',0)\,dx'$$

$$h_{zk}(x,0^-) = \hat{Y}_1 \cdot e_{xk}(x,0) \equiv \int_{-c/2}^{0} Y_1(x,x') e_{xk}(x',0)\,dx'$$

where

$$Y_u(x,x') = \frac{k_t^2}{j\omega\mu}\sum_n \Phi_n(x)\Phi_n(x')\frac{\cot(k_n b)}{k_n}$$

$$Y_1(x,x') = \frac{k_t^2}{j\omega\mu}\sum_n \Phi_n(x)\Phi_n(x')\frac{\cot(k_n d)}{k_n}.$$

The eigenvalue equation for transverse resonance is

$$\left[\hat{Y}_u + \hat{Y}_1\right]\cdot e_{xk} = 0$$

or

$$\frac{k_t^2}{j\omega\mu}\sum_n \Phi_n(x)\langle e_{xk}(x,0);\Phi_n(x)\rangle \frac{\cot(k_n b)+\cot(k_n d)}{k_n} = 0 \tag{1}$$

where

$$\langle e_{xk}(x,0);\Phi_n(x)\rangle = \int_{-c/2}^{0} e_{xk}(x,0)\Phi_n(x)\,dx.$$

The expression for $e_{xk}(x,0)$ is now to be determined. In order to take into account the presence of the edge singularities, we introduce a weight function:

$$W(x) = \frac{1}{\sqrt{1-\left(\dfrac{2x}{c}\right)^2}}$$

in the expansion of the x component of the kth field with unknown amplitudes X_{mk}, namely,

$$e_{xk}(x,0) = W(x)\sum_{m=0,2,4} X_{mk} f_m(x)$$

with $f_m(x)$ proportional to the Chebyshev polynomial, $T_m(x)$:

$$f_m(x) = \sqrt{\frac{2\epsilon_m}{\pi c}}T_m\left(\frac{2x}{c}\right)$$

($\epsilon_{m=0} = 1$, $\epsilon_{m\neq 0} = 2$). Hence

$$\langle e_{xk}(x,0);\Phi_n(x)\rangle = \sum_{m=0,2,4} X_{mk} P_{mn} \tag{2}$$

with

$$P_{mn} = \delta_n\sqrt{\frac{\epsilon_m \pi c}{2a}}(-1)^{m/2} J_m\left(\frac{n\pi c}{2a}\right)$$

where J_m denotes the Bessel function of integer order. The index m stands for $0,2,4,\cdots$ to satisfy the parity of $e_{xk}(x,0)$.

Now, we rewrite (1) using (2). Multiplying (1) by $e_{xp}(x,0)$ and integrating in x, one obtains

$$\frac{k_t^2}{j\omega\mu}\sum_n \langle e_{xk}(x,0);\Phi_n(x)\rangle\langle e_{xp}(x,0);\Phi_n(x)\rangle \cdot \frac{[\cot(k_n b)+\cot(k_n d)]}{k_n} = 0.$$

Introducing matrix notation, we can write the above transverse resonance equation as

$$[Y][X] = 0 \tag{3}$$

with

$$Y_{vm} = \frac{k_t^2}{j\omega\mu}\frac{c}{2}\pi\sum_n \sqrt{\epsilon_m\epsilon_v}\frac{\delta_n^2}{a}(-1)^{(m+v)/2} J_m\left(\frac{n\pi c}{2a}\right)J_v\left(\frac{n\pi c}{2a}\right) \cdot \frac{[\cot(k_n b)+\cot(k_n d)]}{k_n} \tag{4}$$

where X is the vector of the X_m components. Setting $\beta = 0$, the solutions of the equation

$$\det[Y] = 0 \tag{5}$$

give the cutoff frequencies of the TE modes with electric wall ($n = 0,2,4,\cdots$) and magnetic wall ($n = 1,3,5,\cdots$).

B. TM Modes

An analogous development holds for TM modes. In this case, the problem is formulated in terms of $\partial E_z(x,0)/\partial x$, instead of $E_z(x,0)$, because the former has the same singularity as $e_{xk}(x,0)$. Moreover, better convergence of the ad-

mittance operator is obtained by this choice. The fields of the kth mode are

$$e_k(x,y) = -\frac{1}{k_t}\nabla_t \Pi_k(x,y)$$

$$h_k(x,y) = -\frac{1}{k_t}\hat{z}\times\nabla_t \Pi_k(x,y)$$

$$e_{zk}(x,y) = \frac{k_t}{j\omega\epsilon}\Pi_k(x,y)$$

with

$$k_t^2 = k_0^2 - \beta^2 = -\partial_x^2 - \partial_y^2$$

$$\nabla_t^2 \Pi_k(x,y) + k_t^2 \Pi_k(x,y) = 0$$

and the only boundary condition is $\Pi_k(x,y)=0$ at $x=0$, $x=-a$, $y=b$, and $y=-d$. Therefore

$$e_{zk}(x,y) = \frac{k_t}{j\omega\epsilon}\sum_n \Phi_n'(x) I_n \begin{cases} -\dfrac{\sin k_n(y-b)}{\sin k_n b}, & y \geqslant 0 \\ \dfrac{\sin k_n(y+d)}{\sin k_n d}, & y \leqslant 0 \end{cases}$$

$$\Phi_n'(x) = \frac{2\delta_n}{\sqrt{a}}\sin\left(\frac{n\pi}{a}x\right).$$

An electric wall ($n=2,4,6,\cdots$) or a magnetic wall ($n=1,3,5,\cdots$) is placed at $x=-a/2$.

Now, we can expand $\int(\pi/a)h_{xk}(x,y)dx$ in terms of $(a/\pi)\partial e_{zk}(x,0)/\partial x$ and evaluate the Green's admittances:

$$Y_u(x,x') = \frac{j\omega\epsilon}{k_t^2}\sum_n \Phi_n(x)\Phi_n(x')\frac{k_n}{n^2}\cot(k_n b)$$

$$Y_l(x,x') = \frac{j\omega\epsilon}{k_t^2}\sum_n \Phi_n(x)\Phi_n(x')\frac{k_n}{n^2}\cot(k_n d)$$

so that

$$\int \frac{\pi}{a}h_{xk}(x,0^+)\,dx = \hat{Y}_u\cdot\frac{a}{\pi}\frac{\partial e_{zk}(x,0)}{\partial x}$$

$$\int \frac{\pi}{a}h_{xk}(x,0^-)\,dx = \hat{Y}_l\cdot\frac{a}{\pi}\frac{\partial e_{zk}(x,0)}{\partial x}.$$

Setting

$$\left\langle \frac{a}{\pi}\frac{\partial e_{zk}(x,0)}{\partial x};\Phi_n(x)\right\rangle = \sum_{m=2,4} X_{mk}P_{mn}$$

where P_{mn} is as previously defined and now m starts from 2 to satisfy the boundary conditions of the $e_{zk}(x,0)$ field component, the resulting dispersion equation is

$$\left[\hat{Y}_u + \hat{Y}_l\right]\cdot\frac{a}{\pi}\frac{\partial e_{zk}(x,0)}{\partial x} = 0. \tag{6}$$

Again expanding the unknown field in terms of the same basis on the aperture

$$\frac{a}{\pi}\frac{\partial e_{zk}(x,0)}{\partial x} = \sum_{m=2,4} X_{mk} f_m(x) W(x) \tag{7}$$

and introducing matrix notation, the dispersion equation (6) becomes

$$[Y][X] = 0 \tag{8}$$

with

$$Y_{vm} = \frac{j\omega\epsilon}{k_t^2}\frac{c}{2}\pi\sqrt{\epsilon_m\epsilon_v}(-1)^{(m+v)/2}\sum_n \frac{\delta_n^2}{a}J_m\left(\frac{n\pi c}{2a}\right)J_v\left(\frac{n\pi c}{2a}\right)\cdot\frac{k_n}{n^2}\left[\cot(k_n b)+\cot(k_n d)\right]. \tag{9}$$

Setting $\beta=0$ and the determinant of Y to zero, we obtain the cutoff frequencies of TM modes, with electric wall ($n=2,4,6,\cdots$) and magnetic wall ($n=1,3,5,\cdots$). The complete expressions for TE and TM modes are reported in Appendix I.

We have thus determined the complete spectrum of the local section, apart from the fundamental TEM mode. We note that the solution $\beta=k_0$, corresponding to the TEM mode, is contained in (3). By setting $\beta=k_0$, i.e., $k_t=0$, from (A1), we observe that $h_{zk}(x,y)=0$. Thus we can assert that the fundamental mode can be obtained from the TE mode for $\beta=k_0$.

TABLE I
CUTOFF FREQUENCIES WITH ONE, TWO, AND THREE EXPANSION FUNCTION S FOR $a=6.0$ m, $b=d=3.0$ m, AND $w=5.0$ m

Type	1	2	3
$TE_{(even)}$	14.270	14.270	14.270
$TE_{(odd)}$	31.816	31.819	31.819
$TE_{(even)}$	57.373	57.374	57.374
$TE_{(odd)}$	64.082	64.089	64.089
$TE_{(even)}$	79.437	79.451	79.451
$TE_{(odd)}$	94.426	94.558	94.558
$TE_{(even)}$	103.451	103.453	103.453
$TE_{(odd)}$	111.475	111.480	111.480
$TE_{(even)}$	125.116	125.244	125.244
$TE_{(odd)}$	130.395	130.395	130.395
$TE_{(odd)}$	139.797	139.974	139.974
$TE_{(even)}$	144.026	144.052	144.152

TABLE II
CUTOFF FREQUENCIES WITH ONE TWO, AND THREE EXPANSION FUNCTIONS FOR $a=6.0$ m, $b=1.0$ m, $d=3.0$ m, AND $w=5.0$ m

Type	1	2	3
$TE_{(even)}$	19.799	19.980	19.980
$TE_{(odd)}$	38.609	38.611	38.611
$TE_{(even)}$	60.852	60.865	60.865
$TE_{(odd)}$	61.061	61.069	61.069
$TE_{(even)}$	77.203	77.215	77.215
$TE_{(odd)}$	81.551	81.638	81.638
$TE_{(odd)}$	93.806	93.925	93.925
$TE_{(even)}$	104.531	104.658	104.658
$TE_{(odd)}$	107.864	107.864	107.864
$TE_{(even)}$	119.336	119.582	119.582
$TE_{(odd)}$	129.202	129.521	129.521
$TE_{(even)}$	142.208	142.286	142.286

C. Results for a Local Section

We have examined sections with the inner plate in a symmetrical and an asymmetrical position. We report in Table I the results for a symmetrical case and in Table II those for an asymmetrical one. As can be seen, convergence with the number of expansion functions is extremely rapid.

TABLE III
CUTOFF FREQUENCIES IN MHz FOR DIFFERENT SYMMETRICAL ($b = d$) STRUCTURES COMPARED WITH RESULTS OF [4], [5]:
1) $a = 6$ m $a/b = 2.0$ $w/a = 0.83$
2) $a = 25.4$ cm $a/b = 2.0$ $w/a = 0.83$
3) $a = 42.34$ cm $a/b = 3.4$ $w/a = 0.72$
4) $a = 50$ cm $a/b = 3.4$ $w/a = 0.72$

	Present Work	[4]	[5]
1	31.82	32.4	32.0
2	752.72	765.3	755.4
3	595.91	639.0	599.8
4	504.61	541.4	508.1

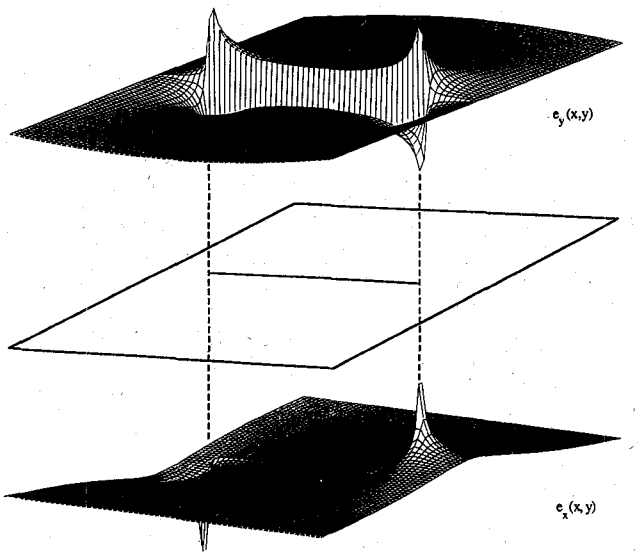

Fig. 3. Transverse components $e_x(x, y)$, $e_y(x, y)$ for the fundamental mode for a section of dimensions $a = 6$ m, $b = d = 3$ m, and $w = 4$ m.

Moreover, we have good agreement with theoretical results obtained in the literature [4], [5], as reported in Table III.

Three-dimensional plots of the transverse components of the fundamental mode are depicted in Fig. 3 for the symmetric case. In this figure, it can be seen that the fields are similar to those of a parallel-plate guide, the effects of the lateral conducting walls being negligible in the middle of the section.

We also report in Fig. 4 3-D plots of the transverse components $e_x(x, y)$ and $e_y(x, y)$ of the first higher mode of the symmetrical case and in Fig. 5 3-D plots of the $e_x(x, y)$ and $e_y(x, y)$ field components for the asymmetrical one. It is evident how boundary conditions, edge conditions, and continuity at the interface are exactly satisfied.

In Fig. 6 are reported the capacitance per unit length of symmetric and asymmetric cross sections. Maintaining the ratios a/b, a/d, and a/w constant along z, the characteristic impedance is always the same. In Fig. 7 the behavior of the equipotential lines of the fundamental mode is reported for a symmetric and an asymmetric case.

III. COUPLING OF THE LOCAL MODES

In the previous section, we determined the complete spectrum of the local uniform section. Now we will use this to determine the propagation along the whole GTEM cell, whose section is variable along z. The dimensions of the

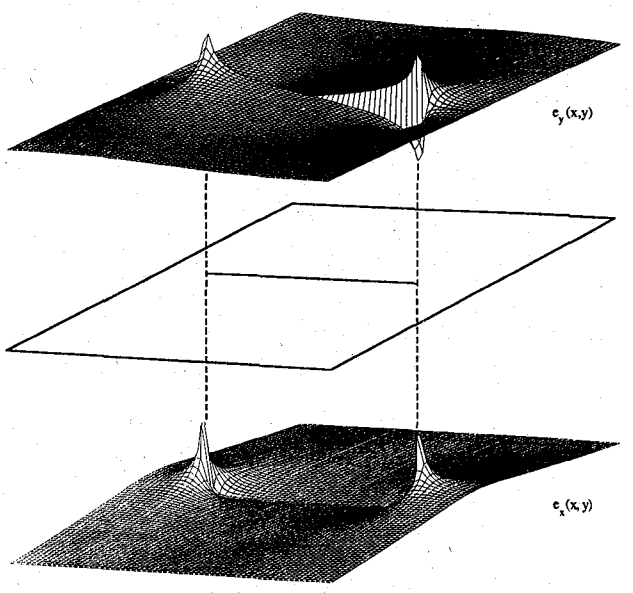

Fig. 4. Transverse components $e_x(x, y)$, $e_y(x, y)$ for the first higher mode for a section of dimensions $a = 6$ m, $b = d = 3$ m, and $w = 4$ m.

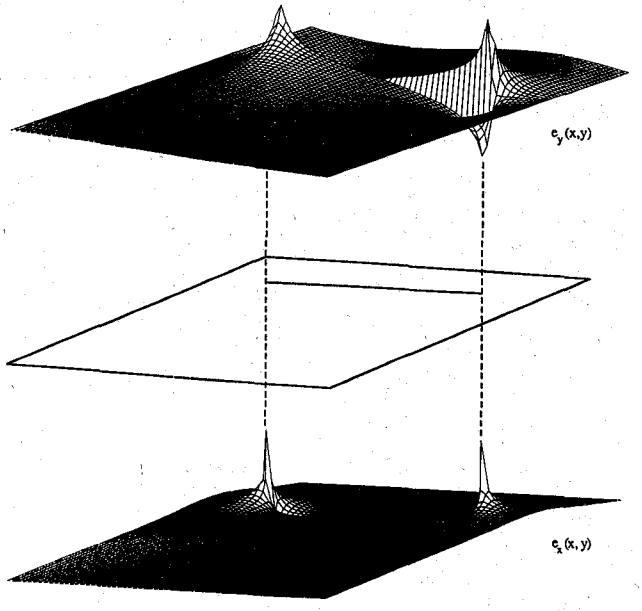

Fig. 5. Transverse components $e_x(x, y)$, $e_y(x, y)$ for the fundamental mode for a section of dimensions $a = 6$ m, $b = 2$ m, $d = 5$ m, and $w = 4$ m.

local section are related to z, as shown in Figs. 8 and 9:

$$a = 2z \tan \alpha \qquad b = z[\tan \gamma - \tan \theta]$$
$$d = z[\tan \gamma + \tan \theta] \qquad c = \rho a$$

with ρ constant along the whole structure.

Starting from the equation of the curl of the electric field [9], we can write

$$\left[\partial_y E_z(x, y; z) - \partial_z E_y(x, y; z)\right]\hat{x} + \left[\partial_z E_x(x, y; z) - \partial_x E_z(x, y; z)\right]\hat{y} + \left[\partial_x E_y(x, y; z) - \partial_y E_x(x, y; z)\right]\hat{z} = -j\omega\mu \boldsymbol{H}. \quad (10)$$

We expand the fields $\boldsymbol{E}_t(x, y; z)$ and $\boldsymbol{H}_t(x, y; z)$ in terms of

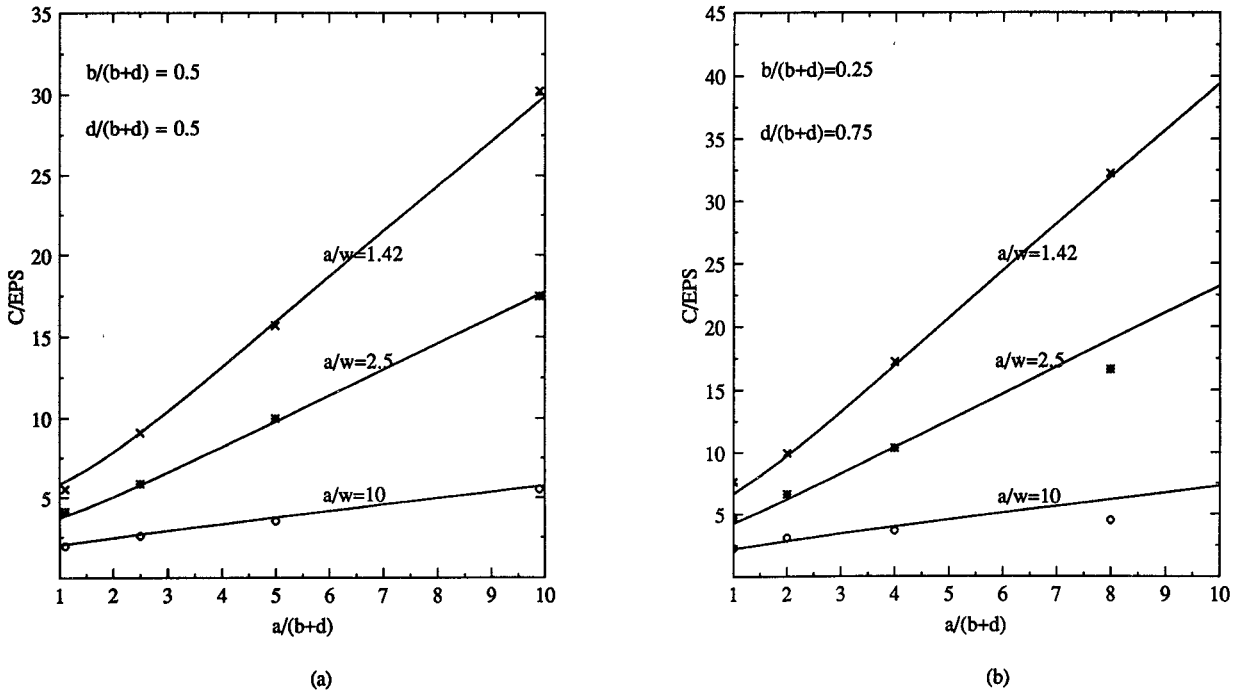

Fig. 6. Capacitance per unit length (C/ϵ_0) of the cross section of the present work (continuous line) compared with [7]: (a) symmetric case; (b) asymmetric case.

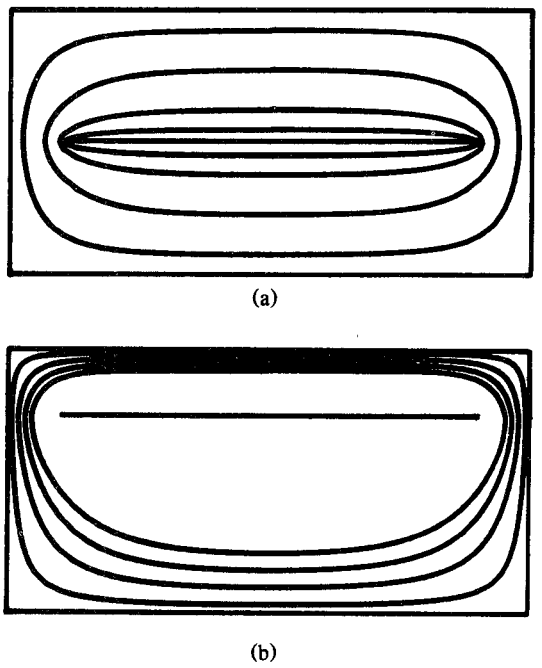

Fig. 7. Equipotential lines in the cross-section for symmetric and asymmetric cases: (a) $a/b = 4$, $a/(b+d) = 2$, $a/w = 1.25$; (b) $a/b = 8$, $a/(b+d) = 2$, $a/w = 1.25$.

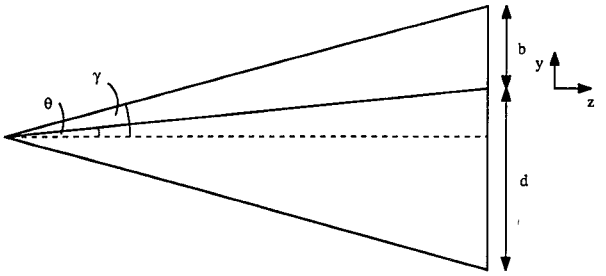

Fig. 8. The $y-z$ section of the GTEM cell.

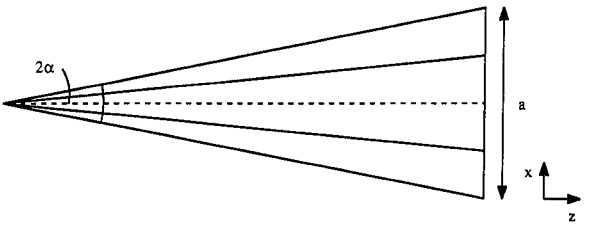

Fig. 9. The $x-z$ section of the GTEM cell.

N local modes of the structure at the plane z:

$$\boldsymbol{E}_t(x,y;z) = \sum_{k=1}^{N} V_k(z)\boldsymbol{e}_k(x,y;z) \tag{11}$$

$$\boldsymbol{H}_t(x,y;z) = \sum_{k=1}^{N} I_k(z)\boldsymbol{h}_k(x,y;z) \tag{12}$$

where $\boldsymbol{e}_k(x,y;z)$ and $\boldsymbol{h}_k(x,y;z)$ are dimensionless fields that are explicit functions of x, y; they implicitly depend on the longitudinal coordinate z and are normalized as

$$\int_s \boldsymbol{e}_k(x,y;z) \times \boldsymbol{h}_p(x,y;z) \cdot \boldsymbol{z}\, ds = \delta_{kp}.$$

Impedances (or admittances) enter in the $V_k(z)$'s and $I_k(z)$'s. The solution of the problem involves evaluating the modes $\boldsymbol{e}_k(x,y;z)$ and $\boldsymbol{h}_k(x,y;z)$ (determined in the previous section) and amplitudes $V_k(z)$ and $I_k(z)$. By (11) and

(12), the transverse component of (10) can be expressed as

$$\partial_y E_z(x,y;z) - \partial_z\left\{\sum_{k=1}^{N} V_k(z) e_{yk}(x,y;z)\right\} = -j\omega\mu \sum_{k=1}^{N} I_k(z) h_{xk}(x,y;z) \tag{13}$$

$$\partial_z\left\{\sum_{k=1}^{N} V_k(z) e_{xk}(x,y;z)\right\} - \partial_x E_z(x,y;z) = -j\omega\mu \sum_{k=1}^{N} I_k(z) h_{yk}(x,y;z). \tag{14}$$

Multiplication of (13) by h_{xp} and (14) by h_{yp} and summing yields

$$\begin{aligned}\sum_{k=1}^{N} \partial_z[V_k(z)]\,[&e_{xk}(x,y;z)h_{yp}(x,y;z) - e_{yk}(x,y;z)h_{xp}(x,y;z)] \\ &= -j\omega\mu \sum_{k=1}^{N} I_k(z)\boldsymbol{h}_k(x,y;z)\cdot\boldsymbol{h}_p(x,y;z) \\ &\quad + \partial_x[E_z(x,y;z)]h_{yp}(x,y;z) - \partial_y[E_z(x,y;z)]h_{xp}(x,y;z) \\ &\quad + \sum_{k=1}^{N} V_k(z)\partial_z[e_{yk}(x,y;z)]h_{xp}(x,y;z) \\ &\quad - \sum_{k=1}^{N} V_k(z)\partial_z[e_{xk}(x,y;z)]h_{yp}(x,y;z). \end{aligned} \tag{15}$$

The spectrum obtained in the previous section satisfies the conditions of vanishing E_z on the boundary and on the inner plate for the uniform structures. In the tapered structure, however, the field component that must vanish is the electric field tangential to the sloping conductors of Figs. 8 and 9. Therefore the boundary conditions on the actual structure are

$$\begin{aligned} E_{\tan}(x,b;z) &= E_{\tan}(x,-d;z) = E_{\tan}(0,y;z) \\ &= E_{\tan}(-a,y;z) = 0 \\ E_{\tan}(x,0;z) &= 0 \quad \text{(on the inner plate)}. \end{aligned}$$

From Fig. 8, we can write the first equation above as

$$E_{\tan}(x,b;z) = E_z(x,b;z)\cos\gamma + E_y(x,b;z)\sin\gamma = 0$$

or

$$E_z(x,b;z) = -E_y(x,b;z)\tan\gamma.$$

Recalling the expansions (11) and (12) for E_y we can write the last equation as

$$E_z(x,b;z) = -\sum_{k=1}^{N} V_k(z) e_y(x,b;z)\tan\gamma = \sum_{k=1}^{N} V_k(z) l_{zk}(x,b;z)$$

with $l_{zk}(x,b;z) = -e_y(x,b;z)\tan\gamma$.

With analogous developments for the other boundary conditions, we can write, in a compact form on the conducting contour,

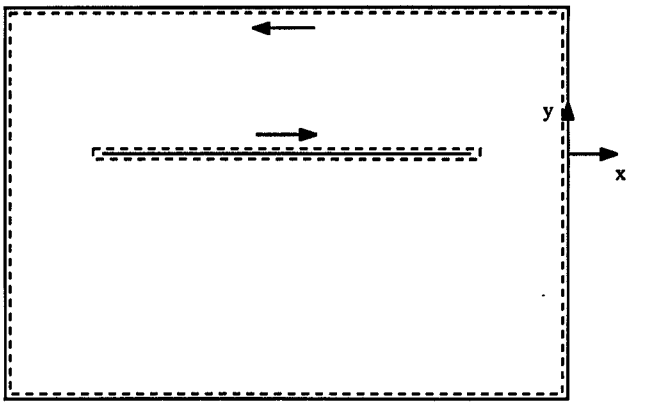

Fig. 10. Integration path in the multiply connected cross section.

$$E_z(x,y;z)|_{\text{contour}} = \sum_{k=1}^{N} V_k(z) l_{zk}(x,y;z) \tag{16}$$

with

$$l_{zk}(x,y;z) = \begin{cases} -e_y(x,y;z)\tan\gamma & \forall x,\ y = b \\ e_y(x,y;z)\tan\gamma & \forall x,\ y = -d \\ e_x(x,y;z)\tan\alpha & \forall y,\ x = -a \\ -e_x(x,y;z)\tan\alpha & \forall y,\ x = 0 \\ -e_y(x,y;z)\tan\theta & \text{on the inner plate.} \end{cases} \tag{17}$$

The complete spectrum we have just determined is complete and orthogonal; thus, it is sufficient to represent arbitrary continuous functions that do not vanish anywhere on the boundary of the structure except on the boundary itself. Imposing the boundary conditions on the sloping conductors produces coupling between the local modes.

Recalling that in a multiply connected surface

$$\int_S f(x,y)\frac{\partial g(x,y)}{\partial_x}\,ds = -\int_S g(x,y)\frac{\partial f(x,y)}{\partial x}\,ds - \int_l f(x,y)g(x,y)\,dy$$

where l comprises the external contour in the anticlockwise direction and the inner contour in the clockwise direction, as shown in Fig. 10, substitution of (16) and (17) in (15) and integration in the cross section yields

$$\partial_z V_k(z) = -\sum_{p=1}^{N} A_{kp}(z)V_p(z) - j\sum_{p=1}^{N} X_{kp}(z)I_p(z), \quad k = 1,2,3,\cdots,N. \tag{18}$$

Analogous developments on the curl of the magnetic field yield

$$\partial_z I_k(z) = -\sum_{p=1}^{N} D_{kp}(z)I_p(z) - j\sum_{p=1}^{N} B_{kp}(z)V_p(z), \quad k = 1,2,3,\cdots,N. \tag{19}$$

Equations (18) and (19) are the telegraphist's equations for

the structure varying along z, with

$$A_{kp}(z) = \int_S \partial_z\left[\boldsymbol{e}_p(x,y;z)\right] \times \boldsymbol{h}_k(x,y;z)\cdot\hat{\boldsymbol{z}}\,ds$$

$$- \int_l l_{zp}(x,y;z)h_{xk}(x,y;z)\,dx$$

$$+ \int_l l_{zp}(x,y;z)h_{yk}(x,y;z)\,dy$$

$$D_{kp}(z) = \int_S \boldsymbol{e}_k(x,y;z) \times \partial_z\left[\boldsymbol{h}_p(x,y;z)\right]\cdot z\,ds$$

$$X_{kp}(z) = \begin{cases} \omega\int_S\left[\mu\boldsymbol{h}_k(x,y;z)\cdot\boldsymbol{h}_k(x,y;z) + \epsilon e_{zk}(x,y;z)e_{zk}(x,y;z)\right]ds, & k=p \\ 0, & k\neq p \end{cases}$$

$$B_{kp}(z) = \begin{cases} \omega\int_S\left[\epsilon\boldsymbol{e}_k(x,y;z)\cdot\boldsymbol{e}_k(x,y;z) + \mu h_{zk}(x,y;z)h_{zk}(x,y;z)\right]ds, & k=p \\ 0, & k\neq p \end{cases}$$

and their expressions are reported in Appendix II.

We observe that (18) and (19) are more general than the classical telegraphist's equations for conventional transmission lines [9], since in addition to the distributed series reactance $X_{kp}(z)$ and shunt susceptance $B_{kp}(z)$, they contain "voltage transfer coefficients" $A_{kp}(z)$ and "current transfer coefficients" $D_{kp}(z)$. These terms take into account power transfer between the "local" modes of a structure that changes along the z direction. Where the change of section is abrupt, power transfer is strong. Moreover, the effect of the enlarging cross section along z is that higher modes become propagating. In GTEM structures with end sections of the order of several square meters, there are many local modes in propagation at frequencies greater than 500 to 700 MHz.

We have solved (18) and (19) taking into account the dependence on z. In particular, for the kth mode, $\beta_k = k_0\sqrt{1-(f_c/f)^2}$, where f_c depends on the dimensions of the section. We have observed that for a structure with all walls varying along z, as shown in Fig. 8 and Fig. 9, the cutoff frequencies of every mode are inversely proportional to z. Then f_c of the kth mode at any section can be evaluated from f_c at the final section, so that

$$\beta_k = k_0\sqrt{1-\left(\frac{z_{\text{end}}f_{ck}}{zf}\right)^2} \tag{20}$$

where f_{ck} is the cutoff frequency of the kth mode at the final section. In this way, at a given frequency f, we can also determine the position where a mode enters into propagation. In the following, the effects of the modes below cutoff are neglected.

IV. Analysis of the GTEM Cell

We have examined how the GTEM cell behaves as a function of frequency, considering $\alpha = 15°$, $\gamma = 10°$, $\theta = 5°$, and $\rho = 0.64$. We report in Fig. 11 the behavior of $|V|$ and $|I|$ versus z for the fundamental mode at 100 MHz. The ratio between $|V|$ and $|I|$ is always the air impedance; moreover, the period is constant. Observing $|V|$ and $|I|$ of the first higher mode (Fig. 12), we notice that they show a variable period along z, due to the variation of β along z of type (20).

A plot of the power distribution along z is reported in Fig. 13. Here the power is carried substantially by the fundamental mode, the higher order local mode entering into propagation only at $z \approx 3$ m.

As reported in Fig. 14, we can observe how the β's of the modes, moving along z, tend to the value k_0, i.e., the propagation constant of a TEM wave. As the frequency is increased, the value k_0 is reached earlier. The kth mode with $\beta_k \approx k_0$ tends to a quasi-planar wave and transfers power with the fundamental mode.

Increasing the frequency, higher local modes enter into propagation at sections closer to the initial one (Figs. 15 and 16). Therefore, coupling between higher order modes occurs, as shown in Figs. 17 and 18. At 700 MHz we note a remarkable amount of power carried by the first higher order local mode; at 1 GHz the power is, instead, distributed over all local modes in propagation, even if we neglect modes greater than the fifth.

V. Conclusions

This work analyzes the GTEM cell, using the concept of "local modes." The cutoff frequencies and the modes of the uniform structure are determined and then applied to the analysis of the structure tapered along z.

In the presence of an object under test in the cell, many local modes are excited. Their amplitudes depend on the object geometry and position and can be evaluated by various methods. This information is required in determining the electromagnetic signature of the object under test. This problem is now under investigation.

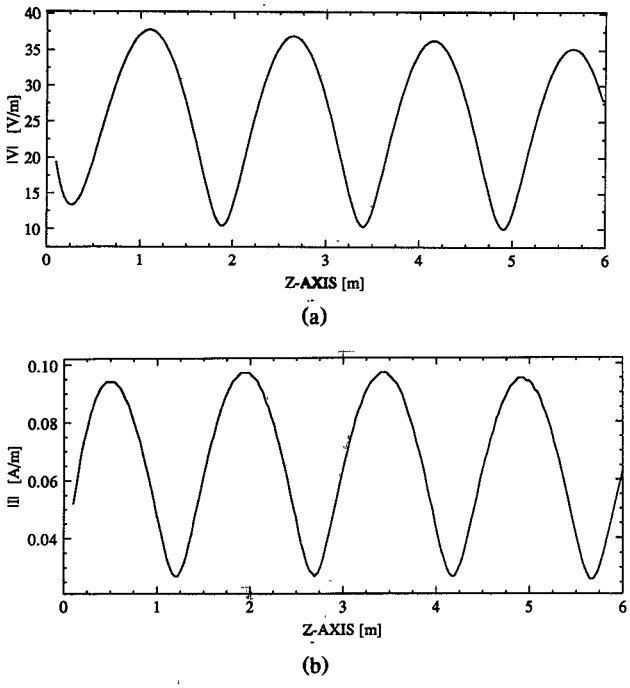

Fig. 11. (a) Behavior of $|V|$ versus z of the fundamental mode. (b) Behavior of $|I|$ versus z of the fundamental mode.

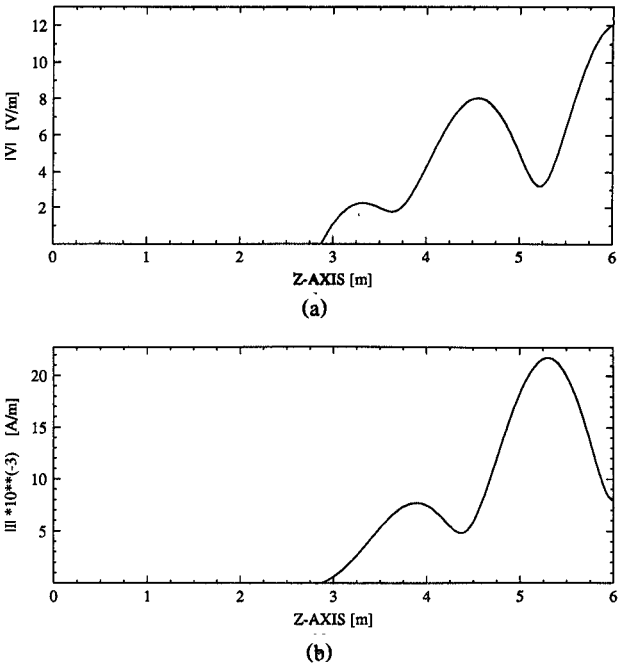

Fig. 12. (a) Behavior of $|V|$ versus z of the first higher mode. (b) Behavior of $|I|$ versus z of the first higher mode.

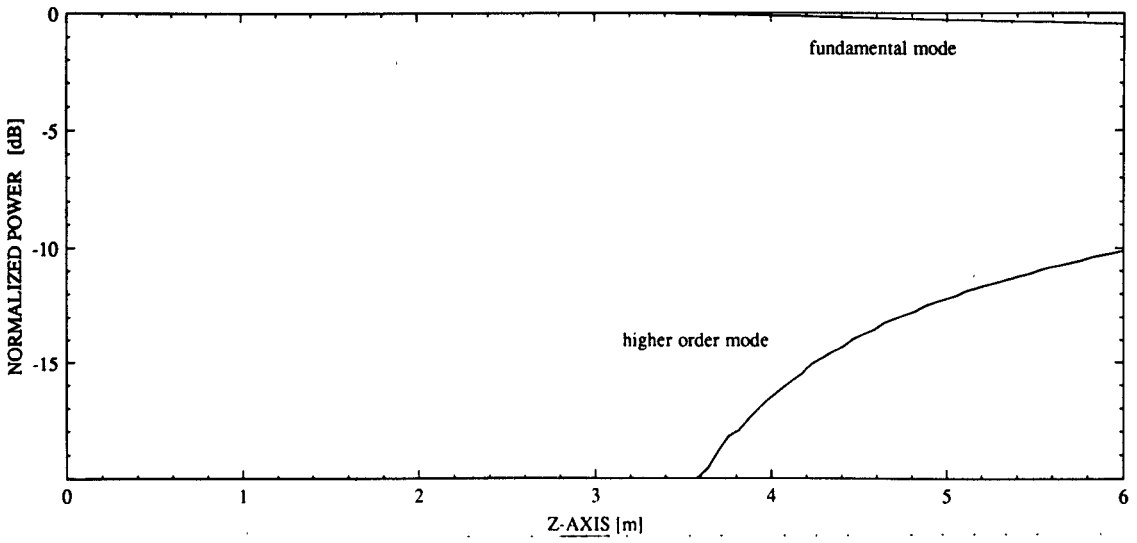

Fig. 13. Power distribution at 100 MHz.

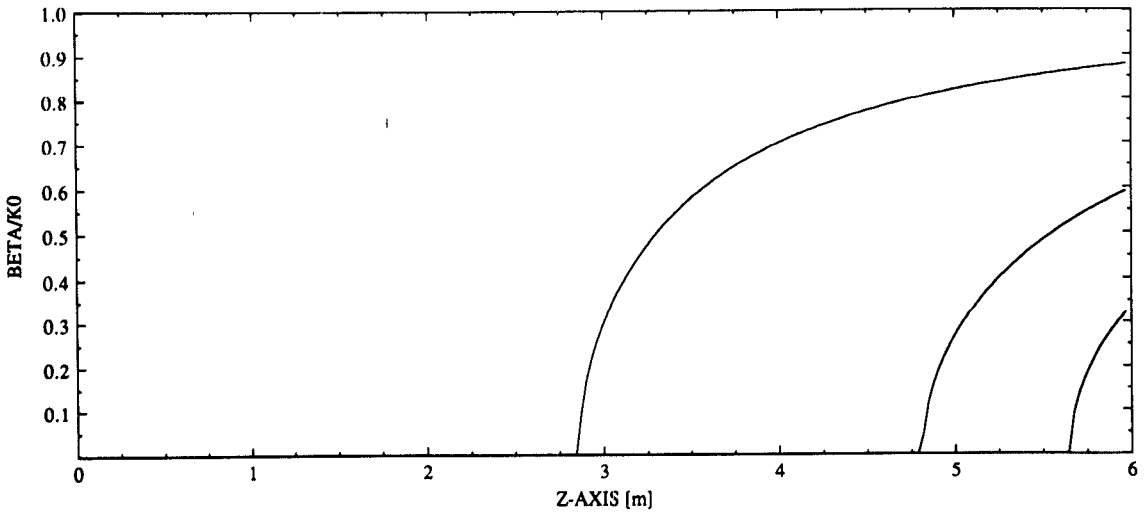

Fig. 14. Behavior of the normalized propagation constants along the z axis of the cell at 100 MHz.

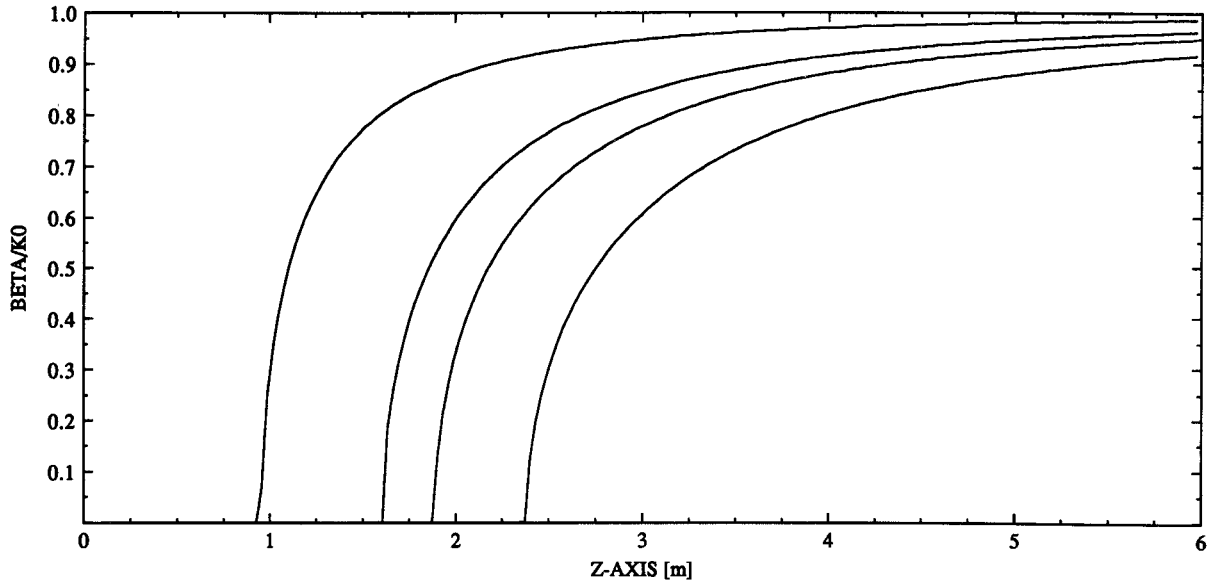

Fig. 15. Behavior of the normalized propagation constants along the z axis of the cell at 300 MHz.

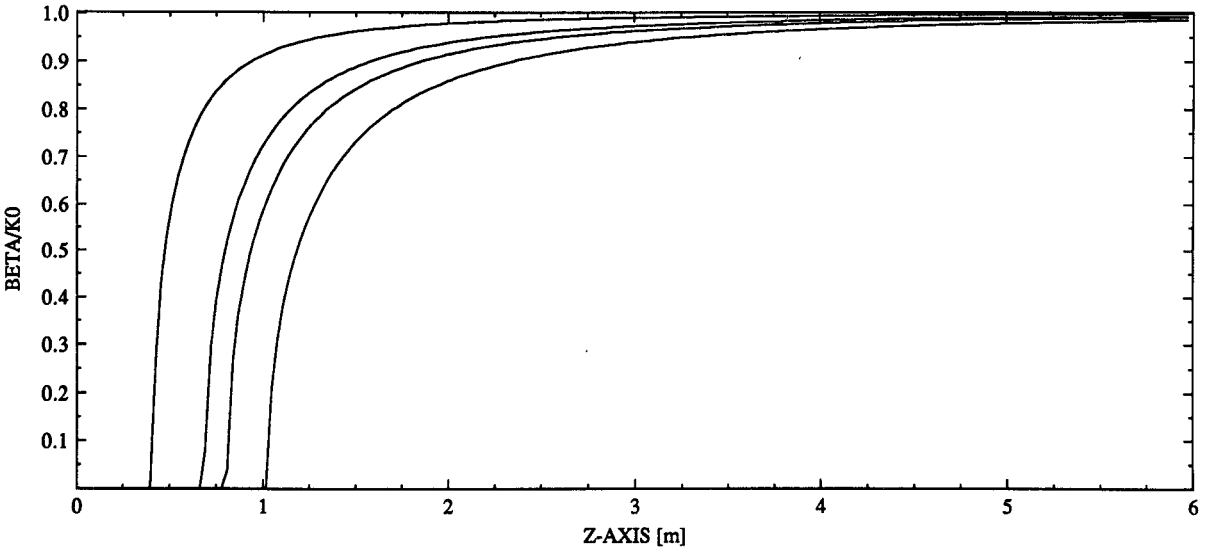

Fig. 16. Behavior of the normalized propagation constants along the z axis of the cell at 700 MHz.

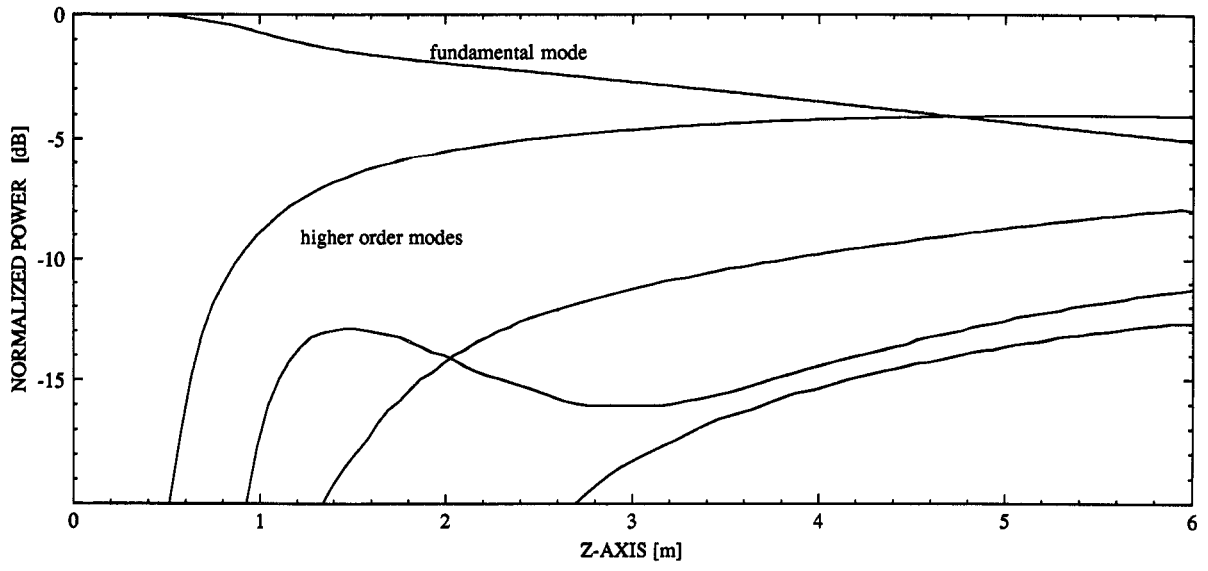

Fig. 17. Power distribution at 700 MHz.

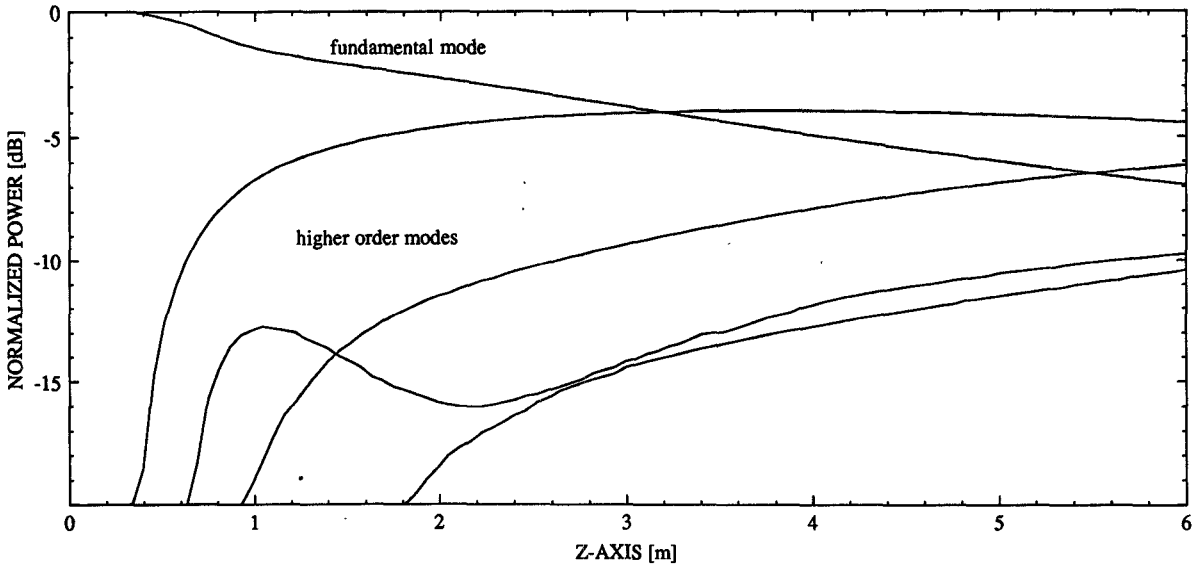

Fig. 18. Power distribution at 1 GHz.

Appendix I

TE

$$e_{xk}(x,y) = h_{yk}(x,y)$$

$$= F_k^{\mathrm{TE}} \sum_{m=0,2,4}^{N} X_{mk} \sum_n P_{mn} \frac{2\delta_n}{\sqrt{a}} \cos\left(\frac{n\pi}{a}x\right)$$

$$\cdot \begin{cases} -\dfrac{\sin k_n(y-b)}{\sin k_n b}, & y \geqslant 0 \\ \dfrac{\sin k_n(y+d)}{\sin k_n d}, & y \leqslant 0 \end{cases}$$

$$e_{yk}(x,y) = -h_{xk}(x,y)$$

$$= F_k^{\mathrm{TE}} \sum_{m=0,2,4}^{N} X_{mk} \sum_n P_{mn} \frac{n\pi}{a} \frac{2\delta_n}{\sqrt{a}} \sin\left(\frac{n\pi}{a}x\right) \frac{1}{k_n}$$

$$\cdot \begin{cases} \dfrac{\cos k_n(y-b)}{\sin k_n b}, & y \geqslant 0 \\ -\dfrac{\cos k_n(y+d)}{\sin k_n d}, & y \leqslant 0 \end{cases} \tag{A1}$$

$$h_{zk}(x,y) = \frac{k_t^2}{j\omega\mu} F_k^{\mathrm{TE}} \sum_{m=0,2,4}^{N} X_{mk} \sum_n P_{mn} \frac{2\delta_n}{\sqrt{a}} \cos\left(\frac{n\pi}{a}x\right) \frac{1}{k_n}$$

$$\cdot \begin{cases} -\dfrac{\cos k_n(y-b)}{\sin k_n b}, & y \geqslant 0 \\ \dfrac{\cos k_n(y+d)}{\sin k_n d}, & y \leqslant 0. \end{cases}$$

TM

$$e_{xk}(x,y) = h_{yk}(x,y)$$

$$= -F_k^{\mathrm{TM}} \sum_{m=2,4}^{N} X_{mk} \sum_n P_{mn} \frac{\pi}{a} \frac{2\delta_n}{\sqrt{a}} \cos\left(\frac{n\pi}{a}x\right)$$

$$\cdot \begin{cases} -\dfrac{\sin k_n(y-b)}{\sin k_n b}, & y \geqslant 0 \\ \dfrac{\sin k_n(y+d)}{\sin k_n d}, & y \leqslant 0 \end{cases}$$

$$e_{yk}(x,y) = -h_{xk}(x,y)$$

$$= F_k^{\mathrm{TM}} \sum_{m=2,4}^{N} X_{mk} \sum_n P_{mn} \frac{k_n}{n} \frac{2\delta_n}{\sqrt{a}} \sin\left(\frac{n\pi}{a}x\right)$$

$$\cdot \begin{cases} \dfrac{\cos k_n(y-b)}{\sin k_n b}, & y \geqslant 0 \\ -\dfrac{\cos k_n(y+d)}{\sin k_n d}, & y \leqslant 0 \end{cases} \tag{A2}$$

$$e_{zk}(x,y) = \frac{k_t^2}{j\omega\epsilon} F_k^{\mathrm{TM}} \sum_{m=2,4}^{N} X_{mk} \sum_n P_{mn} \frac{2\delta_n}{\sqrt{a}} \frac{1}{n} \sin\left(\frac{n\pi}{a}x\right)$$

$$\cdot \begin{cases} -\dfrac{\sin k_n(y-b)}{\sin k_n b}, & y \geqslant 0 \\ \dfrac{\sin k_n(y+d)}{\sin k_n d}, & y \leqslant 0 \end{cases}$$

$$F_k^{\mathrm{TE}} = \left\{ \sum_{m=0,2,4}^{N} X_{mk} \sum_{v=0,2,4}^{N} X_{vk} \sum_n P_{mn} P_{vn} \frac{1}{2k_n} \right.$$

$$\left. \cdot \left[\left(\frac{n\pi}{a}\right)^2 \frac{1}{k_n^2} (f_3 + f_4) + (f_1 + f_2) \right] \right\}^{-1/2}$$

$$F_k^{\mathrm{TM}} = \left\{ \sum_{m=2,4}^{N} X_{mk} \sum_{v=2,4}^{N} X_{vk} \sum_n P_{mn} P_{vn} \frac{k_n}{2n^2} \cdot \left[\left(\frac{n\pi}{a} \right)^2 \frac{1}{k_n^2} (f_1 + f_2) + (f_3 + f_4) \right] \right\}^{-1/2}$$

$$f_1 = \frac{k_n b + \frac{1}{2} \sin 2k_n b}{\sin^2 k_n b} \qquad f_2 = \frac{k_n d + \frac{1}{2} \sin 2k_n d}{\sin^2 k_n d}$$

$$f_3 = \frac{k_n b - \frac{1}{2} \sin 2k_n b}{\sin^2 k_n b} \qquad f_4 = \frac{k_n d - \frac{1}{2} \sin 2k_n d}{\sin^2 k_n d}.$$

When n stands for $0,2,4,\cdots$, the correspondent mode has an electric wall at $x = -a/2$; otherwise it has a magnetic wall.

Appendix II

When modes k and p see the same wall, electric or magnetic, $A_{kp} = A_1 + A_2 + A_3$, $D_{kp} = A_1 + A_2$, with

$$A_1 = \sum_n \sum_{m=0,2,4}^{N} \sum_{i=0,2,4}^{N} \sum_j f_{e_x i}(p,z) f_{h_y m}(k,z) \frac{j\pi}{2az} xsc(j,n) \cdot \begin{cases} G_1(y=b) + G_1(y=d), & \boldsymbol{k \neq p} \\ G_1(y=b) + G_1(y=d), & \boldsymbol{k = p, n \neq j} \\ G_5(y=b) + G_5(y=d), & \boldsymbol{k = p, n = j} \end{cases}$$

$$+ \sum_n \sum_{m=0,2,4}^{N} \sum_{i=0,2,4}^{N} f_{e_x i}(p,z) f_{h_y m}(k,z) \frac{1}{z\zeta_n^2} \cdot \begin{cases} G_2(y=b) + G_2(y=d), & \boldsymbol{k \neq p} \\ \frac{1}{4}[G_5(y=b) + G_5(y=d)], & \boldsymbol{k = p} \end{cases} - \frac{1}{z}\delta_{kp}$$

$$A_2 = \sum_n \sum_{m=0,2,4}^{N} \sum_{i=0,2,4}^{N} \sum_j f_{e_y i}(p,z) f_{h_x m}(k,z) \frac{j\pi}{2az} xsc(n,j) \cdot \begin{cases} -G_3(y=b) - G_3(y=d), & \boldsymbol{k \neq p} \\ -G_3(y=b) - G_3(y=d), & \boldsymbol{k = p, n \neq j} \\ -G_6(y=b) - G_6(y=d), & \boldsymbol{k = p, n = j} \end{cases}$$

$$+ \sum_n \sum_{m=0,2,4}^{N} \sum_{i=0,2,4}^{N} f_{e_y i}(p,z) f_{h_x m}(k,z) \frac{1}{z\zeta_n^2} \cdot \begin{cases} -G_4(y=b) - G_4(y=d), & \boldsymbol{k \neq p} \\ -\frac{1}{4}[G_5(y=b) + G_5(y=d)], & \boldsymbol{k = p} \end{cases}$$

$$A_3 = \tan\theta \sum_n \sum_{m=0,2,4}^{N} \sum_{i=0,2,4}^{N} f_{e_y m}(p,z) f_{h_x i}(k,z) \frac{1}{\zeta_n^2} \cdot \left[-\cot(k_{nk}b)\cot(k_{np}b) + \cot(k_{nk}d)\cot(k_{np}d) \right]$$

$$+ \tan\gamma \sum_n \sum_{m=0,2,4}^{N} \sum_{i=0,2,4}^{N} f_{e_y m}(p,z) f_{h_x i}(k,z) \frac{1}{\zeta_n^2} \cdot \left[\csc(k_{nk}b)\csc(k_{np}b) + \csc(k_{nk}d)\csc(k_{np}d) \right]$$

$$+ \tan\alpha \sum_n \sum_{m=0,2,4}^{N} \sum_{i=0,2,4}^{N} \sum_j f_{e_x m}(p,z) f_{h_y i}(k,z) \cdot (-1)^{n+j} \begin{cases} G_1(y=b) + G_1(y=d), & \boldsymbol{k \neq p} \\ G_1(y=b) + G_1(y=d), & \boldsymbol{k = p, n \neq j} \\ G_5(y=b) + G_5(y=d), & \boldsymbol{k = p, n = j} \end{cases}$$

$$G_1(y) = \frac{\frac{\sin(K_{nk} - K_{jp})y}{(K_{nk} - K_{jp})} - \frac{\sin(K_{nk} + K_{jp})y}{(K_{nk} + K_{jp})}}{\sin(K_{nk}y)\sin(K_{jp}y)}$$

$$G_3(y) = \frac{\frac{\sin(K_{nk} - K_{jp})y}{(K_{nk} - K_{jp})} + \frac{\sin(K_{nk} + K_{jp})y}{(K_{nk} + K_{jp})}}{\sin(K_{nk}y)(K_{jp}y)}$$

$$G_2(y) = \frac{K_{np}}{2\sin(K_{nk}y)\sin(K_{np}y)} \left[-\frac{2K_{nk}y}{(K_{np}^2 - K_{nk}^2)} - \frac{\sin(K_{nk} - K_{np})y}{(K_{nk} - K_{np})^2} - \frac{\sin(K_{nk} + K_{np})y}{(K_{nk} + K_{np})^2} \right]$$

$$G_4(y) = \frac{K_{np}}{2\sin(K_{nk}y)\sin(K_{np}y)} \left[-\frac{2K_{np}y}{(K_{np}^2 - K_{nk}^2)} + \frac{\sin(K_{np} - K_{nk})y}{(K_{np} - K_{nk})^2} - \frac{\sin(K_{nk} + K_{np})y}{(K_{np} + K_{nk})^2} \right]$$

$$G_5(y) = \frac{y - \frac{\sin(2K_{nk}y)}{2K_{nk}}}{\sin^2(K_{nk}y)} \qquad G_6(y) = \frac{y + \frac{\sin(2K_{nk}y)}{2K_{nk}}}{\sin^2(K_{nk}y)}$$

$$xsc(n,j) = \begin{cases} 0, & n = 0 \\ -\frac{a^2}{4n\pi}, & n = j \neq 0 \\ -\frac{a^2}{2\pi}\left[\frac{\cos(n-j)\pi}{n-j} + \frac{\cos(n+j)\pi}{n+j} \right], & n \neq j. \end{cases}$$

The indices n and j in the summations stand for $0,2,4,\cdots$ or $1,3,5,\cdots$, corresponding to electric and magnetic walls respectively.

Instead, when modes k and p do not see the same wall, $A_{kp} = A_3 + A_4$ and $D_{kp} = A_4$, with

$$A_4 = -\sum_n \sum_{m=0,2,4}^{N} \sum_{i=0,2,4}^{N} \sum_j f_{e_{xi}}(p,z) f_{h_{ym}}(k,z) \frac{na}{4z} \cdot \left[\frac{\cos(j-n)\pi}{j-n} + \frac{\cos(n+j)\pi}{n+j} \right] [G_1(y=b) + G_1(y=d)] - \sum_n \sum_{m=0,2,4}^{N} \sum_{i=0,2,4}^{N} \sum_j f_{e_{yi}}(p,z) \cdot f_{h_{xm}}(k,z) \frac{na}{4z} \left[\frac{\cos(n-j)\pi}{n-j} + \frac{\cos(n+j)\pi}{n+j} \right] \cdot [G_3(y=b) + G_3(y=d)], \qquad k \neq p.$$

Here the index n stands for $0,2,4,\cdots$ or $1,3,5,\cdots$, according to whether the kth mode presents an electric or a magnetic wall. The same holds for the index j and the pth mode. Moreover,

$$\frac{1}{\zeta_n} = \frac{2\delta_n}{\sqrt{a}}$$

and

$$f_{e_{xm}}(k,z) = f_{h_{ym}}(k,z) = \begin{cases} F_k^{\mathrm{TE}} X_{mk} P_{mn} \dfrac{1}{\zeta_n} & \text{for TE with electric and magnetic walls} \\ F_k^{\mathrm{TM}} X_{mk} P_{mn} \dfrac{1}{\zeta_n} \dfrac{\pi}{a} & \text{for TM with electric and magnetic walls} \end{cases}$$

$$f_{e_{ym}}(k,z) = f_{h_{xm}}(k,z) = \begin{cases} F_k^{\mathrm{TE}} X_{mk} P_{mn} \dfrac{1}{\zeta_n} \dfrac{n\pi}{k_{nk} a} & \text{for TE with electric and magnetic walls} \\ F_k^{\mathrm{TM}} X_{mk} P_{mn} \dfrac{1}{\zeta_n} \dfrac{k_{nk}}{n} & \text{for TM with electric and magnetic walls} \end{cases}$$

As regards B_{kp} and X_{kp}, we obtain

$$B_{kk} = \begin{cases} \omega\epsilon & \text{for any TM mode} \\ \dfrac{\beta_k^2}{\omega\mu} & \text{for any TE mode} \end{cases}$$

$$X_{kk} = \begin{cases} \omega\mu & \text{for any TE mode} \\ \dfrac{\beta_k^2}{\omega\epsilon} & \text{for any TM mode} \end{cases}$$

$$B_{kp} = X_{kp} = 0, \qquad p \neq k.$$

References

[1] D. Koenigstein and D. Hansen, "A new family of TEM-cells with enlarged bandwidth and optimized working volume," in *Proc. 7th Int. Zurich Symp. and Techn. Exh. on EMC*, Mar. 1987, pp. 127–132.

[2] P. Wilson, D. Hansen, and D. Koenigstein, "Simulating open area test site emission measurements based on data obtained in a novel broadband TEM cell," in *Proc. IEEE 1989 Nat. Symp. EMC* (Denver), May 1989.

[3] D. Hansen, P. Wilson, D. Koenigstein, and H. Schaer, "A broadband alternative EMC test chamber based on a TEM-cell anechoic-chamber hybrid concept," in *Proc. Int. Symp. EMC.* (Nagoya), Sept. 1989.

[4] J. C. Tippet, D. C. Chang, and M. L. Crawford, "An analytical and experimental determination of the cutoff frequencies of higher-order TE modes in a TEM cell," Univ. Colorado, Rep. NBSIR 76-841, June 1976.

[5] R. Mittra and T. Itoh, "A new technique for the analysis of the dispersion characteristics of microstrip lines," *IEEE Trans. Microwave Theory Tech.*, vol. MTT-19, pp. 47–56, Jan. 1971.

[6] J. C. Tippet and D. C. Chang, "Higher order modes in rectangular coaxial line with infinitely thin inner conductor," Univ. Colorado, Rep. NBSIR 78-873, Mar. 1978.

[7] J. C. Tippet and D. C. Chang, "Characteristic impedance of a rectangular coaxial line with offset inner conductor," *IEEE Trans. Microwave Theory Tech.*, vol. MTT-26, pp. 876–883, Nov. 1978.

[8] T. Rozzi and S. J. Hedges, "Rigorous analysis and network modeling of the inset dielectric guide," *IEEE Trans. Microwave Theory Tech.*, vol. MTT-35, pp. 823–833, Sept. 1987.

[9] S. A. Schelkunoff, "Conversion of Maxwell's equations into generalized telegraphist's equations," *Bell Syst. Tech. J.*, pp. 995–1043, Sept. 1955.

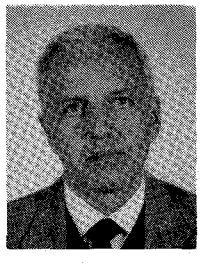

Roberto De Leo was born in Bari, Italy, in 1942. He graduated from the Politecnico di Torino in 1965.

From 1966 to 1980 he was at the University of Bari, working on microwave devices. Since 1980 he has been a Full Professor of Electromagnetics at the University of Ancona, Ancona, Italy. His areas of interest are microwave hyperthermia, optoelectronics devices, and electromagnetic compatibility.

T. Rozzi (M'65–SM'75–F'90) was born in Italy in 1941. He obtained the degree of 'Dottore' in physics from the University of Pisa in 1965, the Ph.D. degree in electronics engineering from Leeds University, England, in 1968, and the degree of D.Sc. from the University of Bath, England, in June 1987.

From 1968 to 1978 he was a Research Scientist at the Philips Research Laboratories, Eindhoven, the Netherlands, having spent one year, 1975, at the Antenna Laboratory of the University of Illinois at Urbana.

In 1975 he was awarded the Microwave Prize by the Microwave Theory and Technique Society of the Institute of Electrical and Electronics Engineers. In 1978 he was appointed to the Chair of Electrical Engineering at the University of Liverpool, and in 1981 he became Chair and Head of the Electronics Group at the University of Bath. From 1983 to 1986 he held the additional post of Head of the School of Electrical Engineering at Bath. Since 1988 Professor Rozzi has held the chair of Antennas and Propagation in the Department of Electronics and Control, University of Ancona, Italy, while remaining a visiting professor at Bath University.

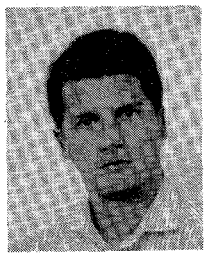

Carlo Svara was born in Ancona, Italy, in 1963. He received the "Doctor" degree in electronic engineering from the University of Ancona in 1989.

Since 1990, he has been with Aeritalia SpA as a researcher. His areas of interest are radar systems and microwaves.

Leonardo Zappelli was born in Rome in 1962. He received the "Doctor" degree in electronic engineering from the University of Ancona in 1987.

Since 1988, he has been with the Department of Electronics and Automatics at the University of Ancona as a researcher assistant. His areas of interest are integrated optics and microwaves.